Vector Control and Experimental Verification of Magnetically Modulated Motor for HEV Application

Toshihiko Noguchi, Sawanth Krishna Machavolu, Yuto Motohashi, and Masahiro Aoyama [†]

Shizuoka University and Suzuki Motor Corporation [†]

noguchi.toshihiko@shizuoka.ac.jp, sawanth.krishna.machavolu.16@shizuoka.ac.jp

Abstract-**Vector control of a magnetically modulated motor (MMM) is described in this paper. The structure of the motor is rather different from a standard permanent magnet synchronous motor (PMSM) because it has two rotors with two different mechanical output shafts, i.e., an outer magnetic-flux modulator and an inner PM rotor. There have been several studies on an electromagnetic field analysis and an optimum design of the motor, but investigation on the vector control using a real machine is still unexplored. Therefore, the paper discusses the vector control algorithm of the MMM and experimentally examines control performance of the mechanical output power delivered by the two rotors, using a prototype machine. Several experimental tests have been conducted under some driving modes, assuming a hybrid electric vehicle (HEV) application. It has been verified that the control algorithm discussed in the paper makes it possible to control the two rotor output power as well as the stator input power like a conventional planetary-gear-based HEV, including the motoring and regenerating modes.**

I. INTRODUCTION

In recent years, studies on a magnetically modulated motor (MMM) are intensively promoted for the purpose of integrating a hybrid electric vehicle (HEV) system with a power split mechanism. The MMM has two rotors, i.e., an outer magnetic flux modulator and an inner permanent magnet (PM) rotor [1], [2]. The former transfers the mechanical power to the drive shaft, and the latter is mechanically coupled with the engine in a standard use. The MMM can synthesize the engine power and the mechanical motor power converted from the input electric power supply, and deliver the synthesized mechanical power to the drive shaft through the modulator. In addition, surplus mechanical power from the engine can be regenerated to the electric power supply through the stator. The stator rotating magnetic flux is modulated by the outer rotor, and the modulated magnetic flux interlinks the inner PM rotor to generate the torque; thus, additional power losses are caused by the interlinking magnetic flux which includes various high frequency components, e.g., eddy current loss in the PM and extra iron losses in the rotor [3]. Therefore, investigations on the optimized configuration of the motor are still conducted using FEM based electromagnetic analysis [4]. In addition, an operation principle and a control algorithm are discussed

due to its electrical and mechanical complexity. However, the detailed vector control (the field oriented control) algorithm has not been explored yet [5].

The authors investigated the basic model of the MMM and its simplified magnetic circuit to derive the voltage equation, which is the basis of the vector control [6]. In addition to that, a prototype has been produced for verification of the operation principle, and some experimental tests have been conducted to simulate the typical HEV driving modes. The vector control is carried out on the basis of the derived voltage equation, focusing on the followings:

1) relationship between the torque and the gear ratio;
2) characteristic between the torque and the current;
3) verification of the derived voltage equation with the experimental results; and
4) power flow of simulated HEV driving modes.

II. VOLTAGE EQUATION OF MAGNETICALLY MODULATED MOTOR

A. Simplified Magnetic Circuit of Basic Model

The MMM to derive the mathematical model has $P_s : P_{pm} : P_{mod} = n : 2n : 3n$ (n is a natural number) relationship, where P_s is a pole pair number of the stator, P_{pm} is the number of the modulator iron cores, and P_{mod} is a pole pair number of the inner PM rotor. The rotor is assumed to be a surface PM structure. Fig. 1 shows a magnetic circuit of the MMM, where $P_s : P_{pm} : P_{mod} = 1 : 2 : 3$ ($n = 1$). In the figure, $\mathcal{R}_s$ is stator back yoke reluctance, $\mathcal{R}_t$ is stator tooth reluctance, $\mathcal{R}_g$ is air gap reluctance, $\mathcal{R}_{mod}$ is modulator reluctance, $\mathcal{R}_r$ is inner PM rotor core reluctance, and $\mathcal{R}_{leak}$ is reluctance corresponding to the total leakage flux. The number of the winding turns is N for each phase.

Fig. 2 is a three-phase magnetic circuit of the MMM. Assuming that $\mathcal{R}_u$, $\mathcal{R}_v$, and $\mathcal{R}_w$ are the total reluctance of the three phases, they can be expressed by the following equation because the reluctance variations of the three phases caused by the modulator are in phase with each other:

$$\begin{aligned} \mathcal{R}_u = \mathcal{R}_v = \mathcal{R}_w = \mathcal{R}_{dc} - \mathcal{R}_{mod}\cos(P_{mod}\theta_{mod}) \\ \because \mathcal{R}_{dc} = \mathcal{R}_g + \mathcal{R}_t + \mathcal{R}_r + \mathcal{R}_s/3 \end{aligned}, \quad (1)$$

where θ_{mod} is a modulator position. Solving the three-phase magnetic circuit shown in Fig. 2, the total number of flux linkage at the phase U coil can be obtained as

$$\psi_u = \left\{ \frac{N^2}{\mathcal{R}_{leak}} + \frac{N^2}{\mathcal{R}_{dc}} + \frac{\mathcal{R}_{mod}N^2}{\mathcal{R}_{dc}^2}\cos(P_{mod}\theta_{mod}) \right\} i_u$$
$$- \frac{1}{2}\left\{ \frac{N^2}{\mathcal{R}_{dc}} + \frac{\mathcal{R}_{mod}N^2}{\mathcal{R}_{dc}^2}\cos(P_{mod}\theta_{mod}) \right\} i_v \qquad . \qquad (2)$$
$$- \frac{1}{2}\left\{ \frac{N^2}{\mathcal{R}_{dc}} + \frac{\mathcal{R}_{mod}N^2}{\mathcal{R}_{dc}^2}\cos(P_{mod}\theta_{mod}) \right\} i_w$$

The self inductance L of each phase and the mutual inductance M can be derived from (2) as follows:

$$L = \ell + L_{dc} + L_{ac}\cos(P_{mod}\theta_{mod})$$
$$M = -\frac{1}{2}L_{dc} - \frac{1}{2}L_{ac}\cos(P_{mod}\theta_{mod}) \qquad . \qquad (3)$$
$$\because \ell = \frac{N^2}{\mathcal{R}_{leak}}, L_{dc} = \frac{N^2}{\mathcal{R}_{dc}}, L_{ac} = \frac{\mathcal{R}_{mod}N^2}{\mathcal{R}_{dc}^2}$$

B. Voltage Equation and Power Flow of Basic Model

The stator pole pair is different from the rotor pole pair in the MMM, which is the most important different feature from common PM motors. Therefore, it is necessary to discuss the voltage equation of the MMM, taking the pole pair number difference between the stator and the rotor into account. The magnetomotive force of the PM for each phase $\mathcal{F}_u$, $\mathcal{F}_v$, $\mathcal{F}_w$ can be expressed as

$$\mathcal{F}_u = \mathcal{F}\cos(P_{pm}\theta_{pm})$$
$$\mathcal{F}_v = \mathcal{F}\cos\left(P_{pm}\theta_{pm} - \frac{2\pi P_{pm}}{3P_s} \right) , \qquad (4)$$
$$\mathcal{F}_w = \mathcal{F}\cos\left(P_{pm}\theta_{pm} - \frac{4\pi P_{pm}}{3P_s} \right)$$

where θ_{pm} is an inner PM rotor position and $\mathcal{F}$ is the maximum value of the PM magnetomotive force.

On the other hand, a three-phase voltage equation of the MMM can be obtained on the stationary reference frame as

$$\begin{bmatrix} v_u \\ v_v \\ v_w \end{bmatrix} = \begin{bmatrix} R & 0 & 0 \\ 0 & R & 0 \\ 0 & 0 & R \end{bmatrix}\begin{bmatrix} i_u \\ i_v \\ i_w \end{bmatrix} + \frac{d}{dt}\begin{bmatrix} L & M & M \\ M & L & M \\ M & M & L \end{bmatrix}\begin{bmatrix} i_u \\ i_v \\ i_w \end{bmatrix} + \frac{d}{dt}\begin{bmatrix} \psi_u \\ \psi_v \\ \psi_w \end{bmatrix}, \quad (5)$$

where R is the stator winding resistance and ψ_u, ψ_v, ψ_w are the number of flux linkage for each phase after magnetic modulation. There is a relationship $\psi_u = L\mathcal{F}_u/N$, for example. By applying Clarke transformation and Park transformation to (5), a two-axis voltage equation can be obtained on the γ-δ rotating reference frame as

$$\begin{bmatrix} v_\gamma \\ v_\delta \end{bmatrix} = \begin{bmatrix} R + pL & -\omega L \\ \omega L & R + pL \end{bmatrix}\begin{bmatrix} i_\gamma \\ i_\delta \end{bmatrix} + \begin{bmatrix} -E_\gamma \\ \omega\sqrt{\dfrac{3}{8}}\dfrac{L_{ac}\mathcal{F}}{N} - E_\delta \end{bmatrix} . \qquad (6)$$
$$\because \omega = P_{mod}\omega_{mod} - P_{pm}\omega_{pm}$$

Through the above calculation process, the Park transformation is carried out by the rotational coordinate transformation using the rotational angle between the stationary reference frame and the rotating reference frame as

$$\theta = \omega t = P_{mod}\omega_{mod}t - P_{pm}\omega_{pm}t = \theta_{mod} - \theta_{pm}, \qquad (7)$$

where ω_{mod} and ω_{pm} are mechanical angular frequencies of the modulator and the inner PM rotor, respectively. As can be
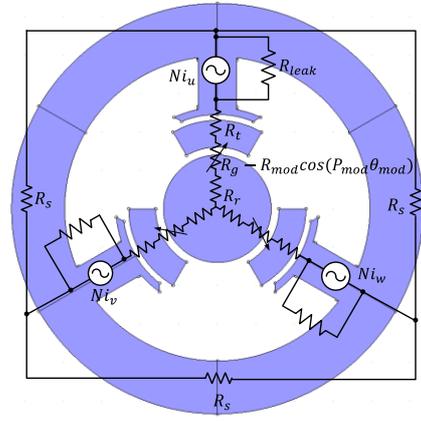

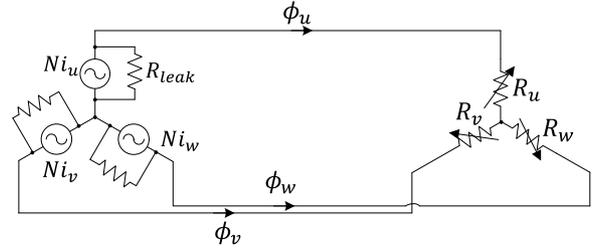Fig. 1. Basic model of MMM and magnetic circuit.

Fig. 2. Three-phase magnetic circuit.

seen in (6), the voltage equation of the MMM is similar to that of the common PM motor on the whole, but extra electromotive forces caused by the asynchronous frequency components are generated as follows:

$$E_\gamma = P_{pm}\omega_{pm}\sqrt{\frac{3}{2}}\frac{(\ell + L_{dc})\mathcal{F}}{N}\sin(P_{mod}\theta_{mod})$$
$$+ (P_{mod}\omega_{mod} + P_{pm}\omega_{pm})\sqrt{\frac{3}{8}}\frac{L_{ac}\mathcal{F}}{N}\sin(2P_{mod}\theta_{mod})$$
$$E_\delta = P_{pm}\omega_{pm}\sqrt{\frac{3}{2}}\frac{(\ell + L_{dc})\mathcal{F}}{N}\cos(P_{mod}\theta_{mod}) \qquad . \qquad (8)$$
$$+ (P_{mod}\omega_{mod} + P_{pm}\omega_{pm})\sqrt{\frac{3}{8}}\frac{L_{ac}\mathcal{F}}{N}\cos(2P_{mod}\theta_{mod})$$

On the other hand, the input electric power can be calculated as follows by using the voltage equation (6):

$$P_i = v_\gamma i_\gamma + v_\delta i_\delta = R(i_\gamma^2 + i_\delta^2) + \omega\sqrt{\frac{3}{8}}\frac{L_{ac}\mathcal{F}}{N}i_\delta$$
$$= R(i_\gamma^2 + i_\delta^2) + \omega_{mod}\tau_{mod} + \omega_{pm}\tau_{pm} . \qquad (9)$$
$$\because \tau_{pm} = -P_{pm}\sqrt{\frac{3}{8}}\frac{L_{ac}\mathcal{F}}{N}i_\delta, \tau_{mod} = P_{mod}\sqrt{\frac{3}{8}}\frac{L_{ac}\mathcal{F}}{N}i_\delta$$

The following torque equation is obtained from (9) and the relationship of the synchronous frequency:

$$\tau_s = \frac{P_s}{P_{pm}}\tau_{pm} = -\frac{P_s}{P_{mod}}\tau_{mod} . \qquad (10)$$

As is described, the MMM corresponds to a planetary gear widely used as a mechanical power splitter, and is capable to distribute the mechanical power among the electric power fed by the inverter, the inner PM rotor, and the modulator.

TABLE I Specifications of Prototype MMM.

Number of stator pole pairs P_s	4
Number of rotor pole pairs P_{pm}	8
Number of modulator cores P_{mod}	12
Stator outer diameter	120 mm
Rotor diameter	61.2 mm
Axial length of core	49.5 mm
Air gap length	0.7 mm
Winding connection	4 series-2 parallel
Maximum current	150 A_{rms}
Armature winding resistance R	33.3 mΩ
Inductance on rotating reference frame L	0.27 mH
Stator flux linkage ψ_a	3.8 mWb

(a) Cross section.   (b) HEV system application.
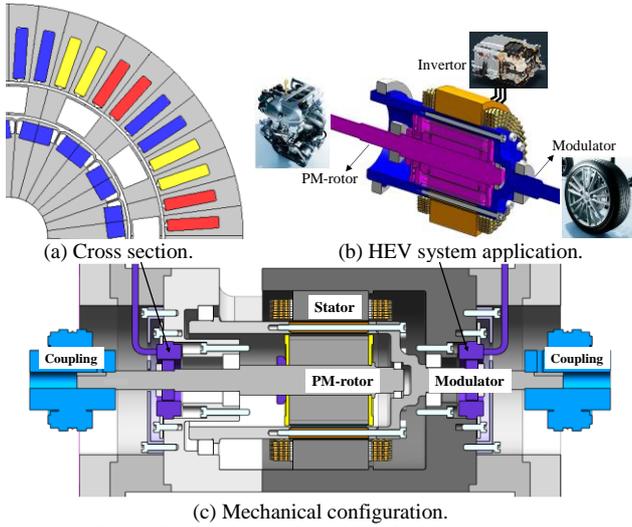

(c) Mechanical configuration.
Fig. 3. Configuration of MMM and HEV application.

III. PROTOTYPE AND EXPERIMENTAL SETUP

Specifications of the prototype MMM are listed in TABLE I. The PM used in the prototype is N39UH (Nd-Fe-B, $B_r = 1.22$ T, $H_{cb} = 965.7$ kA/m@293 K).

Fig. 3 shows a cross section of a motor and the mechanical and electrical connection diagram for a HEV application. The inner PM rotor and the modulator are mechanically connected to the engine and the drive shaft, respectively, and the motor can deliver the torque according to (10) in a motoring mode or a regenerating mode.

Fig. 4 is a photograph of the experimental setup. The two servo motors are connected to the modulator and the inner PM rotor, respectively, and their rotation speeds are controlled independently with two servo amps. The MMM is controlled by a single inverter, and only the torque control is carried out with the vector control. By using two torque meters, two of the mechanical output powers from both shafts can be measured at the same time. The rotation angles of the modulator θ_{mod} and the inner PM rotor θ_{pm} are detected with resolvers mounted on the two shafts, which are used for rotational coordinate transformation in the vector control. Fig. 5 shows a block diagram of the vector control system.
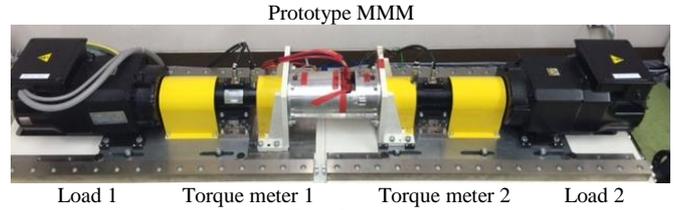
Prototype MMM

Load 1   Torque meter 1   Torque meter 2   Load 2
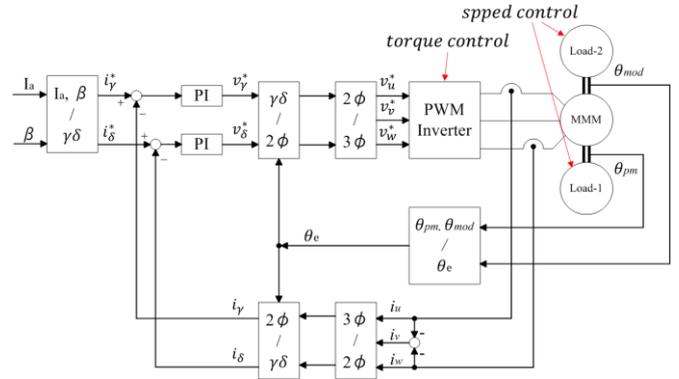Fig. 4. Experimental setup.

Fig. 5. Block diagram of vector control system for MMM.

IV. HEV SIMULATED DRIVING MODES AND OVERVIEW OF EXPERIMENTAL TESTS

A. HEV Simulated Driving Modes

Fig. 6 illustrates three driving modes that simulate HEV operations, where collinear charts and simple power flow diagrams are indicated. The following three driving modes are examined through the experiments:
1) an engine assist mode;
2) an EV mode; and
3) a regeneration mode.

The first test is the engine assist mode, which superimposes the motor output power onto the engine output power, and delivers the synthesized mechanical power to the drive shaft. The second test is conducted under the condition of zero power from the engine, which is called an EV mode. In the mode, the rotating speed of the inner PM rotor is fixed at 0 r/min. The last driving mode is the regeneration mode, where the surplus mechanical power from the engine is regenerated to the inverter through the stator while delivering the mechanical power of the engine to the drive shaft.

B. Overview of Experimental Tests

The following four points are experimentally checked in each driving mode:
1) relationship between the torque and the gear ratio;
2) the torque and current phase angle characteristic;
3) consistency between the voltage equation and the test results; and
4) power flow.

The first point focuses on the relationship expressed by (10). As described previously, the two shafts of the MMM are connected to the two load machines through the torque meters, it is possible to measure the rotating speed and the torque of the modulator and the inner PM rotor without
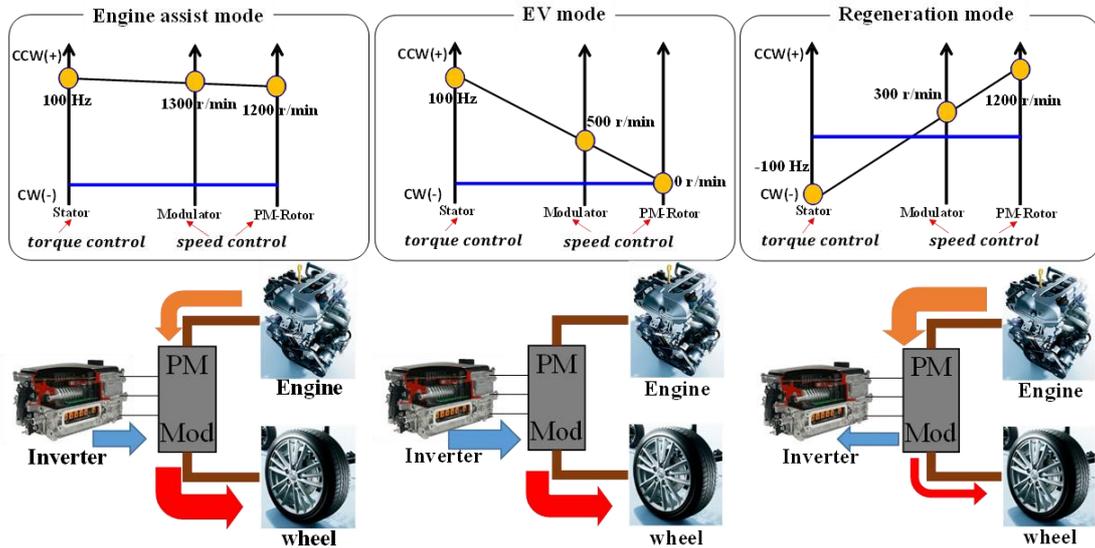
Fig. 6. Driving modes assuming HEV system, collinear charts, and power flow of MMM.

difficulty. On the other hand, the theoretical values of the torque are available from (9), so comparable evaluation is possible between the measured and the theoretical values. The current phase angle β is changed by 15 deg. to check the second point. The third point examines the relationship expressed by (6). This test is carried out by giving the two-axis current commands i_γ^* and i_δ^*, and comparing the theoretical voltages calculated by (6) and the measured values obtained from the controller. Finally, power flow is examined by measuring the input electric power, the output mechanical power, the copper loss, and other losses.

V. EXPERIMENTAL TEST RESULTS

The experimental tests were conducted under the inverter conditions of 80-V DC-bus voltage, 10-kHz switching frequency, 4-μs dead time. The measurement of the torque was performed every 0.5 s to calculate an average value for 15 s of the measured torque. In order to achieve the vector control as accurately as possible, various compensation techniques are implemented in the controller, i.e., dead time compensation, discrete time error compensation, on-voltage compensation of the main switching devices, and so forth [7]. The CCW rotation of the inner PM rotor shaft is defined as a positive direction for both of the torque and the speed.

A. Relationship between Torque and Gear Ratio

Fig. 7 shows the relationship between the torque and the δ-axis current with keeping $i_\gamma = 0$. i_δ is varied every 20 A over the range from 10 to 90 A. It is confirmed from the figure that the torque of the modulator τ_{mod} and the torque of the inner PM rotor τ_{pm} are delivered in proportional to i_δ regardless of the driving modes. As the theoretical equation (10) indicates, the relationship between τ_{mod} and τ_{pm} is

$$\tau_{pm} = -P_{pm}\tau_{mod}/P_{mod} = -2\tau_{mod}/3, \qquad (11)$$

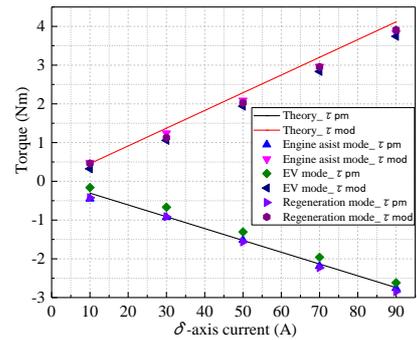which is drawn in the figure as solid lines. The measured τ_{mod} and τ_{pm} agree with the theoretical values well.

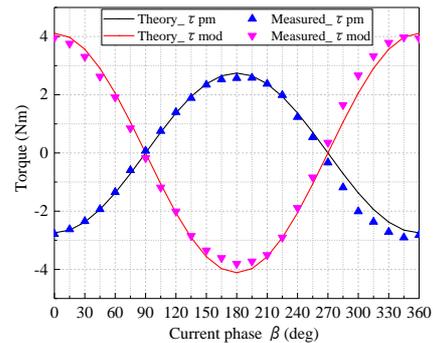Fig. 7. Torque and δ-axis current characteristic.

Fig. 8. Torque and current phase angle β characteristic.

B. Torque and Current Phase Angle Characteristic

The torque and the current phase angle characteristic is shown in Fig. 8, which is measured under the condition of the engine assist mode. The reference phase angle $\beta = 0$ is defined at the δ-axis position, and the current phase angle β is varied every 15 deg. from 0 to 360 deg. The current vector norm is also kept constant at 90 A in the test. Since the prototype has the surface PM structure of the rotor, the similar characteristic to the SPMSM is obtained. As is seen in the figure, the relationship (11) can be confirmed at every measured point, which conforms with the theoretical values.

C. Consistency between Voltage Equation and Test Results

In order to confirm the validity of the voltage equation (6), consistency is examined between the two-axis voltages calculated by (6) and their commands in the controller in the following cases:

1) i_γ is varied under $i_\delta = 0$ condition; and
2) i_δ is varied under $i_\gamma = 0$ condition.

Fig. 9 shows the measured and the theoretically calculated results of the two-axis voltages in the three driving modes. The engine assist mode and the EV mode satisfy the same voltage equation because their phase sequence and their inverter operating frequency are identical.

When $i_\delta = 0$, $v_\gamma = Ri_\gamma$ and $v_\delta = \omega(Li_\gamma + \psi_a)$ from the voltage equation (6), which means that both of the two-axis voltages are proportional to i_γ. On the other hand, substituting $i_\gamma = 0$ into (6), the voltage equations $v_\gamma = -\omega Li_\delta$ and $v_\delta = Ri_\delta + \omega\psi_a$ are obtained, which also means the two-axis voltages are proportional to i_δ. As can be seen in Fig. 9 (a), the two-axis voltages vary almost linearly with the two-axis currents in the both conditions of $i_\delta = 0$ and $i_\gamma = 0$, and the relationships between the voltages and the currents are independent of the driving modes, i.e., the engine assist mode or the EV mode. However, the voltage v_δ in the $i_\delta = 0$ condition and the voltage v_γ in the $i_\gamma = 0$ condition include the inductance L as proportional coefficients. Fig. 9 (a) indicates that L is decreased as the currents goes up due to the magnetic saturation phenomenon, which is confirmed by the significant deviations from the theoretically calculated voltages in higher current ranges. Fig. 9 (b) shows the two-axis voltages in the condition of $i_\delta = 0$ or $i_\gamma = 0$, making the driving mode regenerative operation. The measured results also agree with the theoretical values for any conditions of the two-axis currents even in the regeneration mode; hence, consistency between the voltage equation and the real machine can be confirmed.

Fig. 10 shows the three-phase currents and the two-axis currents in the EV mode and the regeneration mode. The test condition of the EV mode was $i_\gamma = 0$ and $i_\delta = 90$ A, while the regeneration mode was performed under the condition of $i_\gamma = 0$ and $i_\delta = 30$ A. I can be seen in Fig. 9 (a) that the three-phase currents are balanced and sinusoidal waveforms and that the two-axis currents are following their commands with small deviations. On the other hand, similar waveforms of the currents are observed in the regeneration mode shown in Fig. 9 (b). The current waveforms seem to have some ripples, but it should be noted that the vertical axis scale of the graphs is 1/3 of Fig. 9(a); thus, the current control on the rotating γ-δ reference frame is carried out properly. The phase sequence of the three-phase currents is changed to a negative one as shown in Fig. 9 (b) because of the regenerating operation.

D. Power Flow

Fig. 11 shows power flow diagrams in three driving modes assuming the HEV system. The engine assist mode and the EV mode were operated at $i_\gamma = 0$ and $i_\delta = 90$ A, while the regeneration mode was examined at $i_\gamma = 0$ and $i_\delta = 30$ A similar to the case shown in Fig. 10. The test results shown
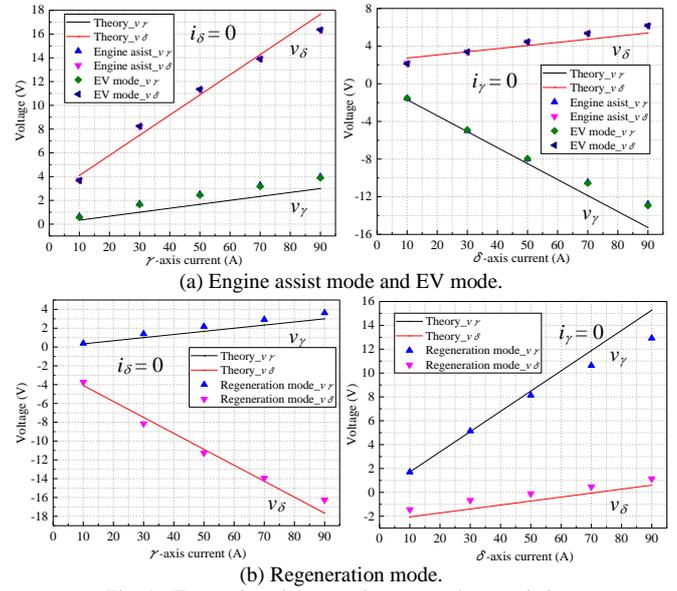

(a) Engine assist mode and EV mode.

(b) Regeneration mode.

Fig. 9. Two-axis voltages and currents characteristics.

(a) Current waveforms in EV mode.

(b) Current waveforms in regeneration mode.
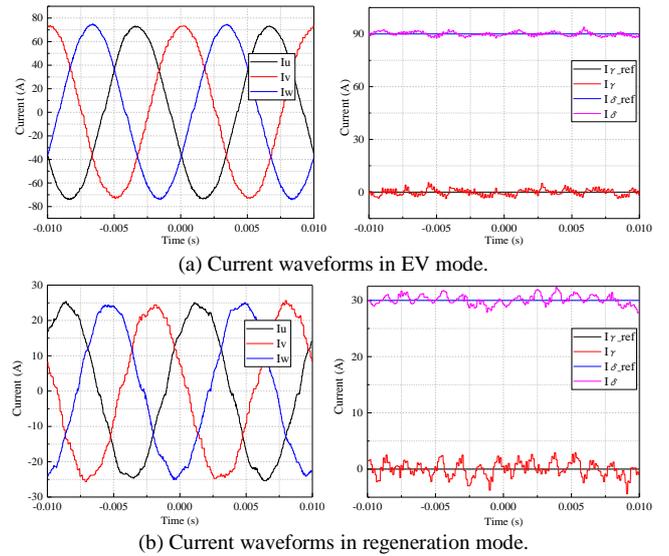
Fig. 10. Current waveforms on stationary and rotating reference frames.

in Fig. 7 indicate that $\tau_{pm} < 0$ and $\tau_{mod} > 0$ when $i_\gamma = 0$ and $i_\delta = 90$ A in the engine assist mode or the EV mode. The collinear chart depicted in Fig. 6 also indicates that the MMM is operated under the $\omega_{pm} > 0$ and $\omega_{mod} > 0$ condition. Therefore, the mechanical power of the inner PM rotor is negative $\tau_{pm}\omega_{pm} < 0$, i.e., the rotor receives the mechanical power from the load machine regarded as the engine, while the mechanical power of the outer modulator is positive $\tau_{mod}\omega_{mod} > 0$, i.e., the modulator delivers its mechanical power to the load machine. In the case, supplemental electric power is provided by the inverter, which is converted to the assist mechanical power for the engine in the MMM.

The rotation speed of the inner PM rotor is zero in the EV mode, which simulates the stopped engine. It is found from Figs. 6 and 7 that $\omega_{pm} = 0$ and $\omega_{mod} > 0$, and that $\tau_{mod} > 0$ when $i_\gamma = 0$ and $i_\delta = 90$ A in this mode. Therefore, the mechanical power of the inner PM rotor is zero, while that of
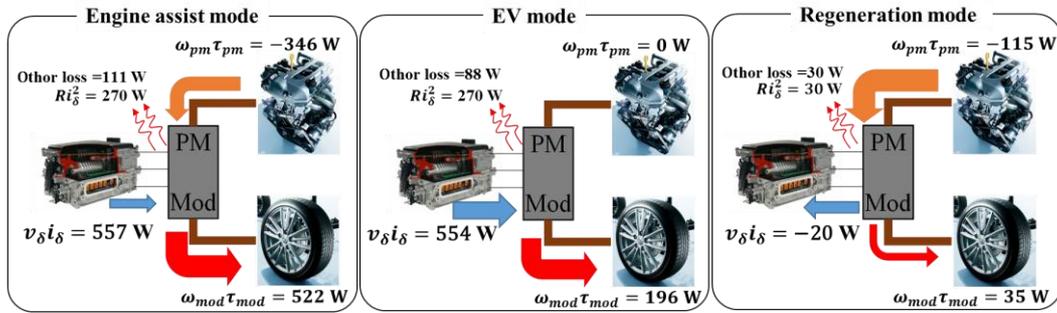
Fig. 11. Power flow of MMM in three driving modes assuming HEV system.

the modulator is positive, which means that the MMM gives the mechanical power to the load machine through the modulator. In the case, the inverter feeds positive electric power to the MMM; hence, it is found that the MMM simply converts the electric power received from the inverter to the mechanical power.

The regeneration mode makes it possible to regenerate the surplus mechanical power of the inner PM rotor to the inverter through the stator windings, transferring the mechanical power to the drive shaft through the modulator at the same time. Negative input electric power from the inverter to the MMM $v_\gamma i_\gamma + v_\delta i_\delta < 0$ is a requirement of the regeneration. As described previously, $v_\delta i_\delta < 0$ is the condition of the regeneration mode because of $i_\gamma = 0$. Fig. 12 shows the result of the input electric power to the MMM by using the measured v_δ. As seen in the figure, the input electric power is negative in the range of the δ-axis current i_δ from 10 to 50 A, which allows the regenerative operation. In fact, the regeneration mode has been achieved when $i_\gamma = 0$ and $i_\delta = 30$ A because the electric power of the inverter is measured negative.

Other losses indicated in Fig. 11 are a residue calculated by the difference between the measured value and the theoretical value. Iron loss and mechanical loss are not included in the voltage equation of (6), so more than 15 % of the total input power seems to be the iron loss and the mechanical loss indicated as other losses.

VI. CONCLUSION

This paper discussed a voltage equation and a torque equation of the magnetically modulated motor. The vector control algorithm has been derived from the voltage equation, and a prototype of the motor has been developed. An experimental system has been set up, and various experimental tests have been conducted with the prototype, assuming three HEV driving modes. Feasibility of the derived voltage equation has been confirmed through the tests, comparing the theoretical values calculated from the equation with the measured two-axis voltages. In addition, it has been confirmed that the torque equation of the motor satisfies a relationship of the gear ratio corresponding to a planetary gear, which can be applied to the power splitter of the HEV system. Furthermore, the power flow has been investigated through the tests based on the three driving modes, and all the
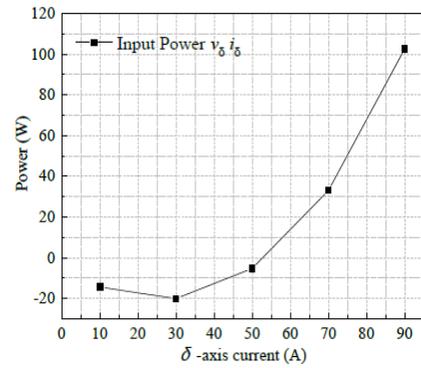

Fig. 12. Input electric power in regeneration mode.

three driving modes are operated properly. It has been found, however, that iron loss of the motor is relatively dominant in the power flow due to the harmonics of the magnetic flux modulated by the outer modulator, which is a future work to improve the motor performance.

The authors intend to analyze the harmonic components caused by the magnetic flux modulation, and to investigate the optimum design of the outer modulator and the inner PM rotor to reduce the motor power losses.

REFERENCES

[1] W. Kaewjinda and M. Konghirun, "A DSP-Based Vector Control of PMSM Servo Drive Using Resolver Sensor," *2006 IEEE Region 10 Conference TENCON*.
[2] C. C. Mi, G. R. Slemon, and R. Bonert, "Minimization of Iron Losses of Permanent Magnet Synchronous Machines," *IEEE Transactions on Energy Conversion*, vol. 20, no. 1, 2005, pp. 121-127.
[3] T. Tonari, H. Kato, and H. Matsui, "Study on Iron Loss of Flux Modulated Type Dual-Axis Motor," *IEEJ Rotating Machinery Technical Meeting*, RM-13-142, 2013, pp. 101-105.
[4] M. Fukuoka, K.Nakamura, H. Kato, and O. Ichinokura, "A Consideration of the Optimum Configuration of Flux-Modulated Type Dual-Axis Motor," *IEEJ Rotating Machinery Technical Meeting*, RM-13-141, 2013, pp. 95-100.
[5] Y. Takeuchi, H. Kato, M. Tago, S. Ogasawara, and H. Sakai, "Operating Principle and Control Method of the Magnetic Modulated Motor," *IEEJ National Convention Record*, No.5-041, 2013, pp. 73-74.
[6] M. Aoyama, Y. Kubota, T. Noguchi, and Y. Motohashi, "Prototype Design of Permanent-Magnet-Free Magnetic Geared Motor for HEV Application," *IEEJ Industry Applications Society Conference*, 3-8, 2015, pp. 97-100.
[7] J. Kudo, T. Noguchi, M. Kawakami, and K. Sano, "Mathematical Model Errors and Their Compensations of IPM Motor Control System," *IEEJ Static Power Conversion Technical Meeting*, SPC-08, 2008, pp. 25-30.